Plasmonic enhancement of single-molecule fluorescence under one- and two-photon excitation

Lu, X.

3

Quantum yield limits for the detection of single-molecule fluorescence enhanced by a gold nanorod

Fluorescence-based single-molecule optical detection techniques are widely chosen over other methods owing to the ease of background screening and better signal-to-noise throughput. Nonetheless, the methodology still suffers from limitations imposed by weak emitting properties of most molecules. Plasmonic nanostructures, such as gold nanorods, can significantly enhance the fluorescence signal of a weak emitter, extending the application of these techniques to a wider range of species. In this work, we explore the lower limit of fluorescence quantum yield for single-molecule detection, using a single gold nanorod to enhance molecular fluorescence. We specifically designed an infrared dye with the extremely low quantum yield of 10^{-4} *and a comparatively large Stokes shift of* $3,000\ \mathrm{cm}^{-1}$ *to demonstrate single-molecule detection by fluorescence enhancement. This example allows us to discuss more general cases. We estimate theoretically the optimal excitation wavelength and the plasmon resonance of the rod which maximize the fluorescence signals. We then confirm experimentally the detection of single-molecule fluorescence with an enhancement factor of* 3 *orders of magnitude for the quantum yield* 10^{-4}*. Theoretical simulations indicate that single-molecule signals should be detectable for molecules with quantum yield as low as* 10^{-6}*, provided the dwell time of the molecules in the plasmonic hot spot is long enough.*

3.1. Introduction

Optical detection of single molecules lies at the core of numerous biochemical studies as it opens up the possibility of investigating individual molecular behaviour usually hidden in the ensemble measurements[1–5]. The key to successful single-molecule detection is to optimize and extract a weak signal from a high background[6–9]. Over the past decades, fluorescence-based single-molecule techniques have been widely applied due to the easy but efficient background suppression and their high sensitivity[9–14]. In this method, the photons emitted at longer wavelength than the excitation light (Stokes-shifted), can easily be discriminated from the background by spectral filtering, providing exceptional contrast and thereby enabling the detection and study of weak single-molecule signals [14, 15]. Notwithstanding the many successes of fluorescence-based single-molecule techniques, it would be important to extend them to a broader range of absorbing molecules with weak emission, especially those emitting in the near-infrared. Chen et.al.[16] have designed deep-red low quantum yield dyes (quantum yield≈0.002) with large Stokes shift that prove to be better in staining mitochondria than normal MitoTrackers. In another work, water-soluble low quantum yield rylene derivative dyes (quantum yield≈0.01) were studied for the application of membrane labelling[17]. They prove to be more photostable than other well-established dyes. While dealing with low-quantum-yield dyes, conventional spectrofluorimeters can not be effectively used to study single-molecule fluorescence mainly because impurities become dominant. The decrease in quantum efficiency for red and NIR dyes is usually attributed to the energy gap law[18]. Recently, the low quantum yield of red fluorescent proteins has been attributed to the presence of dark chromophores[19], which limit their sensing applications [20, 21]. One way to improve these weak emitters is to minimise their nonradiative decay. Another promising strategy to improve the fluorescence efficiency of single-molecule fluorescence is to enhance the radiative emission rate by coupling the fluorophores to plasmonic structures, which can enhance the local field by confining the electromagnetic energy to volumes well below the diffraction limit[2, 13, 22–26].

Compared to strong emitters, poor emitters with low quantum yields benefit from a stronger fluorescence enhancement by plasmonic structures. They are easier to detect at the single-molecule level because of reduced background from unenhanced molecules. This has led researchers in previous studies to employ quenching agents such as methyl viologen [27–29] and nickel chloride[30] to reduce the quantum yield of the emitter. The plasmonic structures in those experiments were fabricated by various top-down and bottom-up approaches. Fluorescence enhancement of emitters with quantum yield down to 1×10^{-3} has been experimentally demonstrated with nano-fabricated bow-tie antennas[31, 32]. More convenient alternative plasmonic structures are wet-chemically synthesized gold nanorods (GNRs), which have attracted significant interest for their facile synthesis and unique optical properties [25, 33–35]. The collective oscillations of the GNR's free electrons, known as localized surface plasmons, strongly confine the electromagnetic field into a sub-wavelength region near the tips, thereby enhancing the excitation rates of the molecules nearby[24]. The plasmonic resonance of GNRs can easily be tuned from the red to the near-infrared range by adjusting their aspect ratio, making them a good single-molecule detection platform for a wide range of fluorescent species[25]. In addition to the excitation enhancement, GNR can enhance radiative channels by increasing the local density of photon states. However, this

enhancement of spontaneous emission is generally accompanied by enhanced non-radiative decay channels. Going closer to the metal will generally increase the excitation and radiative enhancements, but at the same time it will also increase the non-radiative processes responsible for fluorescence quenching, leading to an optimal range for the total enhancement [36–38]. Overlapping the excitation wavelength and the plasmon resonance with the emission spectra of a particular emitter can enhance both the excitation and emission rates, thereby improving the fluorescence enhancement. By using this strategy, we have earlier reported the detection of gold-nanorod-enhanced single-molecule fluorescence from dyes with a quantum yield of 10^{-3}, with an enhancement factor of up to 1000[25]. In the present work, we explore the possibility to enhance the fluorescence of dyes with even lower quantum yield, while keeping the fluorescence observable against background, the strongest source of which is the intrinsic photoluminescence of gold, also enhanced by the plasmon resonance. When going to weaker quantum yields, it is not enough to consider the enhancement factor alone. Indeed, the quantity determining the detection limit is the signal-to-noise ratio, which depends in a complex manner on the plasmon enhancement, the molecular absorption cross section and the fluorescence quantum yield. Therefore, we undertook careful theoretical and experimental investigations of fluorescence enhancement for weak quantum yields in view of optimizing the enhanced fluorescence signal and of extending single-molecule techniques to a much broader range of emitting species.

In this study, we explore single-molecule detection of very weak emitters with quantum yields as low as 1×10^{-4}, by enhancing their fluorescence with a single gold nanorod. To optimize the signal, we need to consider the molecule's Stokes shift (about $150\ \mathrm{nm}$ or $3000\ \mathrm{cm}^{-1}$). Indeed, we have a trade-off between molecular excitation rate and the fluorescence enhancement. Using theoretical simulations, we optimize the excitation wavelength and the plasmon resonance of the rod. We then apply these parameters to detect single-molecule fluorescence experimentally with enhancement factors of three orders of magnitude. We further investigate the quantum yield dependence of the signal-to-noise ratio of the plasmon-emitter coupled system and estimate the lowest quantum yield for which single emitters can be detected in the near field of a single gold nanorod. Although we consider only single nanorods here because of their ease of synthesis, modeling, and manipulation, our results can easily be extended to more complicated nanostructures with much higher near-field enhancement, such as strongly coupled gold nanoparticle dimers or clusters.

3.2. Results and discussion

In this work, instead of selecting molecules with small Stokes shifts (i.e., separation between the maxima of absorption and emission) as done in previous studies[25], we focus on the case of low-quantum-yield dyes, which often have much larger Stokes shifts. For large Stokes shifts (i.e., for small overlaps between the absorption and emission spectra), enhancing both the excitation and the radiation processes with the same narrow-band GNR antenna is very difficult. As a consequence, detection of such single molecules becomes harder than those with small Stokes shifts. To get maximum signals, we will have to sacrifice a fraction of the enhancement factor. In a simple coupled system of a single gold nanorod and an emitter, we can optimize emission by balancing excitation and radiative enhancements, through adjustment of the excitation wavelength and of the aspect ratio of the gold nanorod.

For our study, we selected a molecule of the donor-acceptor type based on Naphthalene Diimide-terthiophene (NDI-2TEG-3T) because it is a very weak emitter. It has a measured quantum yield of about 1.3×10^{-4} and has a large Stokes shift between the emission and the absorption bands. The structure of the molecule is shown in the inset of Figure 3.2.c and the synthesis details are given in the Supporting Information. The low fluorescence efficiency of NDI-2TEG-3T is due to its typical donor-acceptor structure. The introduction of terthiophene units as donors provides an energy level which is suitable for the photoinduced electron transfer process. This extra channel for nonradiative exciton relaxation consequently quenches the fluorescence[39, 40]. When measured in toluene, the NDI-2TEG-3T molecule shows two distinct absorption bands. One of these two bands is assigned to a high-energy $\pi - \pi^*$ transition in the range of 300 to 400 nm. The second one is a low-energy broad intramolecular charge-transfer transition in the range of 500 to 700 nm with its maximum at 590 nm. It originates from the electron-rich terthiophene group to the electron-deficient NDI unit. We focus on the second band with the maximum at 590 nm as it overlaps better with typical gold nanorod resonances. The fluorescence band lies in the near-infrared range with its maximum at about 740 nm. Both bands can be overlapped with the plasmon resonance of gold nanorods, opening possibilities of very large fluorescence enhancements through the combination of excitation and emission enhancements. However, as mentioned before, we need to explore the dependence of the enhanced fluorescence signal on excitation wavelength and on plasmon resonance in order to optimize it.

We begin our discussion with the simulation of fluorescence enhancement of NDI-2TEG-3T by a single gold nanorod. For simplicity, we consider the molecule to lie on the long symmetry axis of the rod, at a variable distance from the tip (we call this distance the 'gap' as represented in the inset of Figure 3.1.b). Considering the small quantum yield and the short lifetime of NDI-2TEG-3T molecules, we apply the simplified two-level scheme model for the calculation of the fluorescence enhancement factor, which neglects the excitation saturation (see Supporting Information for more details). Moreover, we assume both the excitation wave polarization and the molecular dipole to be oriented along the same longitudinal nanorod axis. This simulation therefore applies to the configuration providing maximum enhancement. The plasmon wavelength of the nanorod was tuned by changing its length while keeping its diameter constant at 25 nm, which is the average rod diameter in our experiments. The dielectric permittivity of gold was taken from Johnson and Christy[41], and the refractive index of the medium was set to 1.496 for toluene.

Figure 3.1.b shows the dependence of the excitation and emission enhancements on the gap, with the excitation and plasmon wavelengths at 671 nm and 673 nm, respectively. The excitation enhancement increases monotonously as the gap decreases. The emission enhancement, however, presents a maximum, found here at the gap of about $d_{\mathrm{m}} = 1.5$ nm. The maximum emission enhancement reaches about 200, leading to a maximum total enhancement of five orders of magnitude. The value of d_{m} depends on the dye quantum yield. For quantum yields such as 1×10^{-2}, the optimal gap is about 4 nm (See Figure. S3.11.), whereas for very low quantum yields, the optimal gap shifts to values of 1.5 nm or less (1.5 nm for a yield of 1.3×10^{-4} in Figure 3.1b.). This is because, by reducing the gap, we can benefit from higher excitation and radiative enhancements, while quenching by the metal is still dominated by non-radiative relaxation within the molecule.

Next, we optimized the fluorescence intensity of the nanorod-molecule system, by vary-

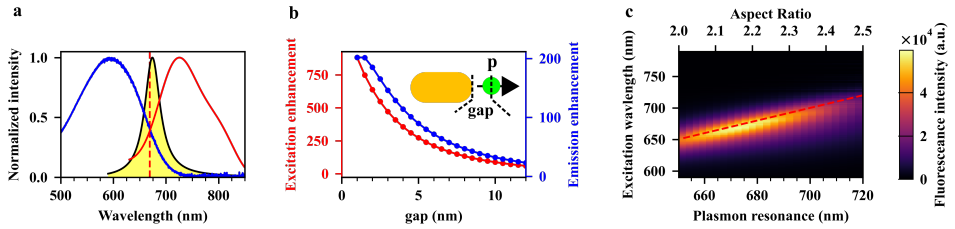

Figure 3.1: (a) Absorption (blue) and emission (red) spectra of NDI-2TEG-3T in toluene. The shaded band is the gold nanorod scattering spectrum calculated for the aspect ratio corresponding to the optimum normalized intensity (see (c)), at excitation wavelength 671 nm (vertical red dashed line). (b) Calculated excitation (red) and emission (blue) enhancements as functions of the gap, i.e., the separation of the molecule from the tip of the gold nanorod. [Inset: schematic of the simulated molecule-nanorod system.] (c) Estimated enhanced fluorescence intensity as a function of the excitation wavelength and of the plasmon resonance wavelength of the gold nanorod. The fluorescence intensity was normalized by the non-enhanced intensity of the fluorescence excited at 671 nm. The red dashed straight line corresponds to the molecule being excited at the wavelength of the plasmon resonance. All values are obtained by varying the gap and selecting the gap value providing maximum enhancement.

ing both the excitation wavelength and the aspect ratio of the gold nanorod. Figure 3.1.c gives the normalized fluorescence intensity as a function of the excitation wavelength and of the resonance wavelength of the gold nanorod. To obtain this plot, we have varied the gap value to optimize the intensity, for each excitation and plasmon wavelength. The plot is given for a fixed quantum yield of 1.3×10^{-4}, corresponding to NDI-2TEG-3T in toluene. As can be seen on Figure 3.1.c, the maximum fluorescence intensity enhanced by each rod is obtained for excitation nearly in resonance with the plasmon, i.e., ($\omega_{\mathrm{exc}} \sim \omega_{\mathrm{sp}}$), because most of the enhancement arises from the excitation. Here ω_{exc} is the frequency of the excitation light source and ω_{sp} is the frequency of the surface plasmon resonance. Next, we note an intensity maximum (sweet spot) at the plasmon wavelength of about 674 nm, which balances the enhancement of both excitation and radiative processes. The total fluorescence enhancement value at this spot is 50,000 times. Here, we can see in Figure 3.1.a that the plasmon resonance at the sweet spot (yellow shaded band) does not overlap exactly with the emission maximum of the molecule, as had been postulated in previous studies to give maximum total fluorescence enhancement (see Supporting Information.), but corresponds to the maximum overlap with both the dye absorption (blue line) and emission (red line) spectrum.

We can interpret the results of simulations in Figure 3.1.c in a very simple way. We notice that the total intensity in Eq (S3.10) is a product of the molecular absorption cross setion C_{abs}, the excitation enhancement factor, and the emission enhancement which is nearly equal to the radiative enhancement factor in the limit of very weak quantum yields. As the excitation and radiation processes are both enhanced by the same narrow plasmon resonance (Lorentzian form), we can approximate the enhanced intensity as:

$$I(\omega_{\mathrm{exc}}) \propto C_{\mathrm{abs}}(\omega_{\mathrm{exc}}) \cdot F_{\mathrm{dye}}(\omega_{\mathrm{exc}}) \cdot f(\omega_{\mathrm{exc}}), \tag{3.1}$$

which means we tune the plasmon resonance and the excitation wavelength to the maximum overlap between absorption and emission of the molecule (see extensive mathematical justification in the Supporting Information).

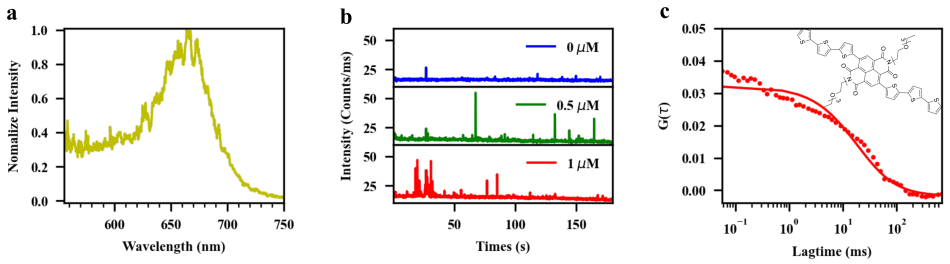

Figure 3.2: (a), Photoluminescence spectra of the gold nanorod deposited on a glass surface and immersed in toluene, which was used to enhance the fluorescence of NDI-2TEG-3T, (b), Photoluminescence time trace from the single gold nanorod immersed in a solution of NDI-2TEG-3T in toluene with different concentrations. (c), The measured (red dashed line) autocorrelation curve of the fluorescence bursts shown in (b) for molecular concentration of 1 μM, and the single exponential fitting of the curve (red solid line). Inset: chemical structure of NDI-2TEG-3T.

We performed fluorescence enhancement experiments on NDI-2TEG-3T molecules under the theoretically derived optimum conditions. Gold nanorods, with average plasmon wavelength of 614 nm, were immobilized on the surface of clean coverslips and immersed in toluene containing different concentrations of NDI-2TEG-3T. The plasmon wavelength of the gold nanorod red-shifts to about 680 nm in toluene due to its high refractive index of 1.496. The measurements were performed on a home-built confocal microscope setup. A circularly polarized continuous-wave (CW) laser with the wavelength of 671 nm was chosen as the excitation source, and was focused by an oil immersion objective with a numerical aperture (NA) of 1.4 to a diffraction-limited spot (about half-a-μm in diameter). A long-pass filter ($\geq$ 675 nm LongPass U-Grade 671/RazorEdge, Semrock) was used to separate the fluorescence signal from the background of scattered laser light. Before adding the NDI-2TEG-3T solution, we recorded photoluminescence (PL) spectra of each bright spot to make sure that the nanoparticle under study had the single Lorentzian lineshape of a single gold nanorod. Time traces were taken for each nanorod under different concentrations of the molecules while keeping the excitation power constant. In each step, the concentration of the molecules was adjusted by adding a certain amount of high concentrated NDI-2TEG-3T solution (50 μM) sequentially, followed by some 10 minutes for diffusion to homogenize the concentration. As confirmed by bulk measurements of the concentration-dependent absorbance, NDI-2TEG-3T is very well dissolved in toluene in our experimental range of molecular concentration (see Figure S3.5). The absence of spectral signatures from dimers and higher clusters confirms that the molecules are well separated from each other, and hence access the plasmonic hot spot independently of each other.

Figure 3.2 shows typical experimental measurements of single-molecule fluorescence enhanced by a single gold nanorod. We first identify single nanorods among spots in the optical image from their photoluminescence spectrum which has a Lorentzian shape and is relatively narrow. Figure 3.2.a indicates a single nanorod with its plasmon resonance at 667 nm. In the intensity time traces as shown in Figure 3.2.b, the background arises from gold nanorod photoluminescence and from the very weak non-enhanced fluorescence of all the molecules in the volume of the excitation focal spot, while the bursts are due to the en-

hanced fluorescence of the molecules within the hot spots near the tips of the rod. To verify that the bursts indeed arise from single molecules, we compared the time traces taken at different NDI-2TEG-3T concentrations. As shown in Figure 3.2.b, in pure toluene solvent, we do not see any strong bursts in the fluorescence time-trace. Bursts appear more and more frequently in the time traces as we increase the NDI-2TEG-3T concentration, while the background remains at a similar level. This observation confirms that the signal from all the non-enhanced molecules in the focal spot (about 52 molecules) is negligible compared to the photoluminescence of the rod, even though the molecular concentration is as high as $1.0\ \mu\mathrm{M}$, because the quantum yield of NDI-2TEG-3T is exceedingly weak. The bursts arise from molecules diffusing through, or being transiently stuck in the tiny hot spots near the tips of the nanorods. The probability of such bursts increases as the molecular concentration increases. By analyzing the highest bursts in the fluorescence time trace, we see the typical single-step single molecule bursts with the time duration in the order of $10\ \mathrm{ms}$ (Figure S3.9), which confirms that only a single molecule was present in the hotspot during the burst, and indicated that it was transiently immobilized. The autocorrelation curve for the fluorescence bursts corresponding to molar concentration of $1\ \mu\mathrm{M}$ is shown in Figure 3.2.c. By fitting the autocorrelation curve to a single exponential, we obtained an average correlation time of $27\ \mathrm{ms}$, which is obviously too long to be due to the free diffusion of molecules through the near field of a nanorod according to the previous works[24–26], where passivation of the glass surface completely suppressed the long-lived bursts. The correlation time results from an interplay between sticking time and bleaching time in the experimental conditions. Here, it can most likely be considered as the result of the transient sticking of dye molecules. Noting that sticking to the metal surface would lead to complete quenching of the fluorescence[42–44], we assign the long bursts to sticking onto the glass substrate. The intensities of the bursts in the time traces depend on the orientation and spatial position of the molecules with respect to the gold nanorods during their residence within the hot spot. As an approximation, we represented the maximum enhanced fluorescence as the largest intensity of the bursts in the time trace, subtracting the background[45]. Those maximum bursts are around $55\ \mathrm{counts/ms}$, whereas the background is $16\ \mathrm{counts/ms}$. To get the enhancement factor, we evaluated the fluorescence signal of one NDI-2TEG-3T molecule from a high-concentration solution ($50\ \mu\mathrm{M}$), by recording the fluorescence signal under the same experimental conditions but on an area without a nanorod. Figure S3.7 (of the Supporting Information) shows such a trace with an average count of 36 per 1 ms bin time, when the excitation power is 3.3 times larger than the power we used for single molecules measurements. We estimate the number of molecules in the focal volume (about $0.061\ \mathrm{fL}$), at the given concentration of $50\ \mu\mathrm{M}$, to be about $1,800$ at any given time. From this, we get an estimate of the average intensity of about $6 \pm 1\ \mathrm{counts/s}$ per molecule. This corresponds to an enhancement factor of about $13,000$, taking the circularly polarized excitation into account. Note that the enhanced signal being stochastic, we estimate it by the largest observed signal, which entails an error of roughly a factor 2. The obtained enhancement value is significantly lower than the best enhancement factor expected for this low quantum yield (more than $100,000$, see Fig 3.3a. hereafter). Various factors can explain the difference: i) the plasmon resonance was not perfectly tuned to the laser and dye wavelengths; ii) the orientation of the molecule was probably not optimal as chosen in the calculation; and, most importantly, iii) the position of the dye was probably on the glass slide and not along the

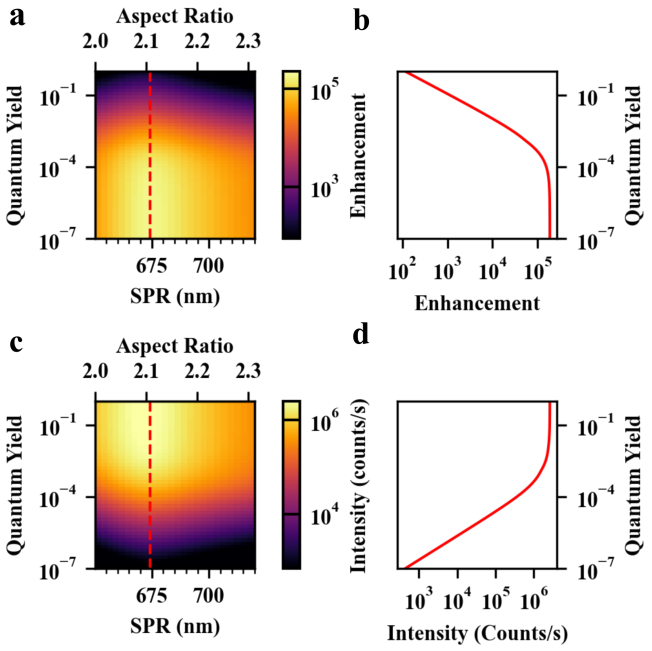

Figure 3.3: (a, c) Simulated fluorescence enhancement (a) and the estimated photon counts (c) from emitters with different quantum yields as functions of the plasmon resonance of the gold nanorod. The excitation wavelength was set as 671 nm. (b, d) Corresponding enhancement factor and emitted intensity enhanced by gold nanorod with the optimized plasmon wavelength of 673 nm (dashed red lines in a and c) as functions of the quantum yield of the molecule. In this plot, we kept the molecular absorption cross section and the excitation intensity constant, i.e., equal to the intensity used in the NDI-2TEG-3T measurements.

rod axis, which is the best position for enhancement. The latter factor can lead to significant reduction of the enhancement factor[46].

To illustrate how the enhancement factor can been tuned by the plasmon resonance of gold nanorods, we examined the fluorescence time traces recorded on gold nanorods with different plasmon wavelengths (see figure. S3.10.). From figure. S3.10. we can see that, as the SPR of the gold nanorods is detuned from the laser (blue shift from 667 nm to 638 nm), the strongest fluorescence bursts in the time traces also decreasing, with the enhancement factors decreasing from about $13,000$ to about $4,000$, respectively.

According to the aforementioned studies, we learn that by properly choosing the wavelengths of the excitation light and the plasmon resonance, we are able to detect single-molecule fluorescence enhanced by a single gold nanorod with high signal-to-background ratio, even though the molecular quantum yield is as low as 1.3×10^{-4}. To gain further insight into the possibility of fluorescence enhancement of single molecules with a simple individual gold nanorod, we performed numerical simulations of the detection limit for molecules with very low quantum yields, keeping the same molecular absorption cross section as NDI-2TEG-3T. In this study, we must consider which background sources will compete with enhanced fluorescence and prevent the detection of single events. Neglecting ex-

perimental imperfections, two sources of background as intrinsic to the sample under study: i) Fluorescence of molecules out of the hot spot. Although the concentration of molecules can exceed a micromolar, their fluorescence is negligible (less than 300 cps) because of the dye's low quantum yield. ii) Photoluminescence of the gold nanorod itself. Although intrinsic gold photoluminescence is very weak (10^{-10})[47], the photoluminescence signal is also enhanced by the plasmon resonance and cannot be separated from the enhanced fluorescence. A typical PL rate for the NRs in this study was $10\ \mathrm{kcps}$. We therefore base our discussion of the signal-to-background ratio on this value.

Figure 3.3 gives the simulated single-molecule fluorescence enhancement by a single gold nanorod as a function of molecular quantum yield. For the sake of comparison, we used the same excitation wavelength $671\ \mathrm{nm}$, the same absorption cross section, and the same fluorescence spectrum as those of NDI-2TEG-3T we used in our measurements. Therefore, the enhanced radiative and metal-induced non-radiative rates are independent of the quantum yields, and they share the same spectral dependence on the plasmon resonance. Because the spectral dependence of the plasmon-dependent emission enhancement is not changed, the spectral position of the plasmon resonance with maximum enhancement is conserved, independently of the quantum yield (see Eq. (S3.9)). As shown in Figure 3.3.a,c, the spectral position of the maximum enhancement factor and of the maximum enhanced fluorescence intensity do not change for different quantum yields. All are located at $674\ \mathrm{nm}$ (dashed red line in Figure 3.3.a,c). At the optimal plasmon wavelength of $674\ \mathrm{nm}$, the total enhancement factor increases dramatically at first, as the quantum yield of the emitter decreases (see Figure. 3.3.d), until it approaches the constant value of 2×10^5, which confirms the simple expression in Eq. (S3.9) for the emission enhancement limit. To understand this result, we approximate the product of excitation and radiative enhancements $\xi_{\mathrm{exc}} \cdot \xi_{\mathrm{rad}}$ (i.e., the total fluorescence enhancement factor expected for vanishing quantum yield) as the fourth power of the field enhancement factor: $\xi_{\mathrm{total}} \xrightarrow{\eta_0 \to 0} \xi_{\mathrm{exc}} \cdot \xi_{\mathrm{rad}} \propto |\mathbf{E}/\mathbf{E}_0|^2 \cdot |\mathbf{E}/\mathbf{E}_0|^2 \sim |\mathbf{E}/\mathbf{E}_0|^4$, the value of which is $(27)^4 \sim 5 \times 10^5$. The enhanced fluorescence intensity, however, drops with the quantum yield as can be seen by substituting Eq.(S3.9) into Eq.(S3.10). The enhanced intensity (see Figure 3.3.d) at first is approximately constant down to a quantum yield of about 10^{-3}, as the decrease in molecular quantum yield is roughly compensated by an associated increase in enhancement. However, when the molecular quantum yield becomes lower than 10^{-3}, the enhancement factor saturates, causing the intensity to drop with the molecular quantum yield. As shown in Figure 3.3.d, the estimated photon intensity from a single emitter drops from $2 \times 10^6\ \mathrm{counts/s}$ to $4 \times 10^3\ \mathrm{counts/s}$ when its quantum yield η_0 decreases from 100% to 10^{-6}. Such a signal would still be detectable above the photoluminescence background of the nanorod, even for an integration time as short as $10\ \mathrm{ms}$. From the above discussion, we find that by enhancing the fluorescence with a single gold nanorod, one can expect photon intensities of thousands of counts/s from a single molecule even though its quantum yield is as low as 10^{-6}, a single-molecule fluorescence comparable with the background from the luminescence of a single gold nanorod ($\sim 10^4\ \mathrm{counts/s}$), under typical excitation laser power in the experiments. However, sufficiently long integration times are needed (about 10 ms), which requires a high medium viscosity, or transient sticking of the molecules. In principle, this contrast allows us to detect the signal from a single molecule. By looking at the signal-to-noise ratio in Figure 3.4, we can see that $SNR \sim 10$ for molecules with the quantum yield of 10^{-6} (green dashed), and even though

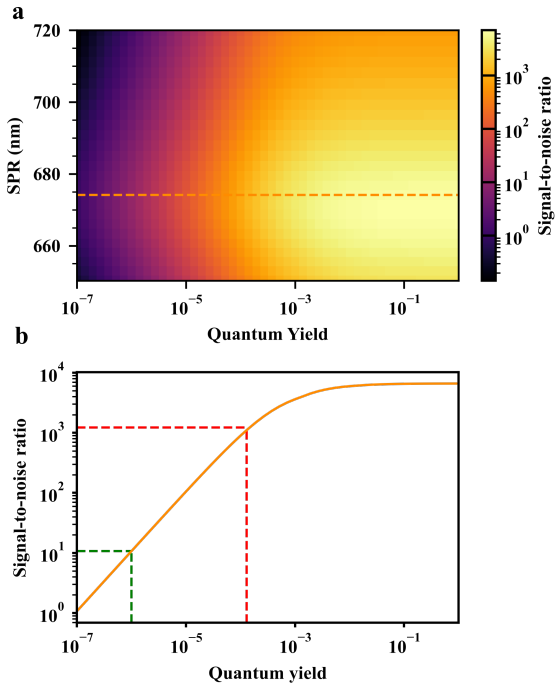

Figure 3.4: (a) Signal-to-noise ratio of the coupled nanorod-molecule system with different plamsonic resonance as functions of the molecular quantum yields. (b) Corresponding signal-to-noise ratio with the the excitation wavelength at 671 nm and the plasmon resonance of the gold nanorod optimizing for the properties of NDI-2TEG-3T (dashed orange line in (a)). We assumed a typical experimental background of nanorod photoluminescence (10^4 cps) at the plasmonic wavelengh of 673 nm, and the photoluminescence of other plasmonic wavelengths were normalized by their scattering cross sections. Integration time was set as 0.1 s. The green dashed line corresponds to molecule of quantum yield 10^{-6} and the red dashed line corresponds to the quantum yield of NDI-2TEG-3T molecule (1.3×10^{-4}).

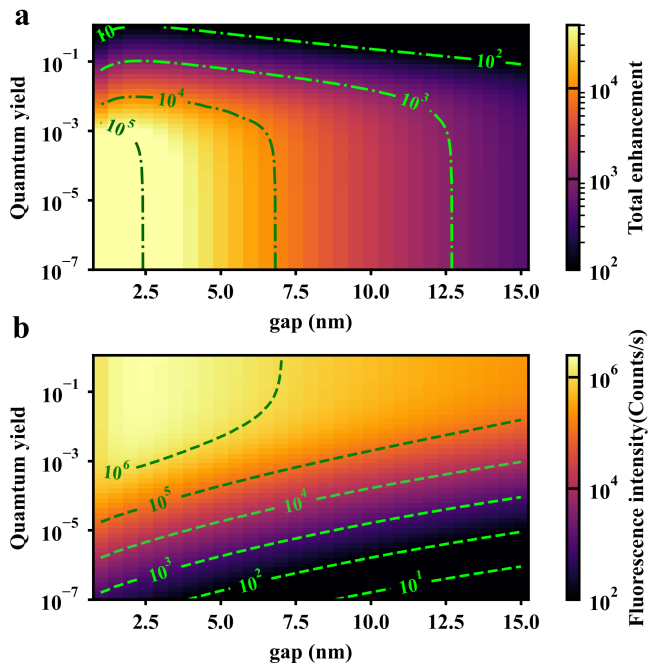

Figure 3.5: Color plots of the calculated fluorescence enhancement (a) and of the estimated photon intensity (b) as functions of the separation of the rod tip to emitter distance (gap) and of the emitter's quantum yield. The green dashed lines in each figure are contours of equal enhancements and intensities. All molecular parameters except the yield were kept constant, as above.

it is one hundred times smaller than that of the measured NDI-2TEG-3T molecules with the quantum yield of 1.3×10^{-4} (red dashed), it still provides enough contrast to distinguish single-molecule signals from background noise.

Following the above discussion, one should keep in mind that as the quantum yield decreases, the volume for the single-molecule fluorescence to be effectively enhanced will also decrease. This can be understood intuitively. As we reduce the quantum yield of the molecule, internal conversion will outcompete quenching by the metal at shorter and shorter distance, so that the molecules can get closer to the gold nanorod and reach larger fluorescence enhancement. This increase of the enhancement can mitigate, to some extent, the strong fluorescence reduction due to the decreasing quantum yield. This partial compensation is seen clearly on the green dashed lines in Figure 3.5, which scales more favorably than quantum yield for small gaps. Therefore, the molecules with smaller quantum yield can get closer to the tips of the nanorod to emit more photons. As a consequence, because diffusion time scales as the squared distance, successful detection of single molecules with very small quantum yield requires slower diffusion or longer binding events than molecule with high quantum yields. Moreover, the reduced effective near-field volume leads to a lower number of detected events, which can be compensated by increasing the concentration of the molecules. We made use of this compensation in our experiment, as we used molecu-

lar concentrations in the μM range instead of nM, as was done in the previous work with quantum yield of 10^{-2}. Additionally, we could also make sure to keep the molecules for longer times in the vicinity of the nanorod tips. This can be done either by slowing down the molecular diffusion in a more viscous solvent, or by transient binding of the molecules within the effective near-field volume, for example through DNA-transient binding[48].

In conclusion, we have provided a detailed study of single-molecule fluorescence enhancement by wet-chemically synthesized single gold nanorods, for extremely weak emitters. The molecule we studied, NDI-2TEG-3T, was specifically designed to emit in the near-infrared range, but with a very low quantum yield of 1×10^{-4}, and a large Stokes shift of 150 nm. Our work provides a suitable demonstration of single-molecule fluorescence enhancement by a single gold nanorod. Our numerical simulations show that, in order to optimize count rates from molecules with low quantum yield and large Stokes shift, we need to optimize the excitation wavelength and the plasmon resonance of the gold nanorod. Based on our theoretical study, we successfully detected single-molecule fluorescence bursts with enhancement factors of up to 10^4 with a simple gold nanorod. The squeezing of the effective near-field volume for enhancement of low-quantum-yield dyes allows us to detect single-molecule signals from solutions of high molecular concentrations, in the range of μM, with high contrast. Theoretical analysis further shows that even for quantum yields as low as 10^{-6}, we will still be able to detect single molecules by fluorescence enhancement by a single gold nanorod, provided the residence time in the effective near-field is longer than tens of ms. The experimental method and the theoretical model presented in this work can be readily extended to other plasmonic nanostructures, which may promote single-molecule techniques based on fluorescence enhancement to a wider range of applications.

S3.1. Supporting information

S3.1.1. Experimental Details

Synthesis and Characterization
Reagents
All reagents and solvents were commercial and were used as received. [2,2':5',2"-terthiophen]-5-yltributylstannane and 2-(2-(2-ethoxyethoxy)ethoxy)ethanamine were synthesized according to literature procedures[49, 50]
Characterization
^{1}HNMR and ^{13}CNMR were performed on a Varian Unity Plus (400 MHz) instrument at 25 ^{o}C, using tetramethylsilane (TMS) as an internal standard. NMR shifts are reported in ppm, relative to the residual protonated solvent signals of $CDCl_3$ (δ= 7.26 ppm) or at the carbon absorption in $CDCl_3$ (δ = 77.23 ppm). Multiplicities are denoted as: singlet (s), doublet (d), triplet (t) and multiplet (m). High Resolution Mass Spectroscopy (HRMS) was performed on a JEOL JMS 600 spectrometer. FT-IR spectra were recorded on a Nicolet Nexus FT-IR fitted with a Thermo Scientific Smart iTR sampler.

Synthesis of NDI-2TEG-3T

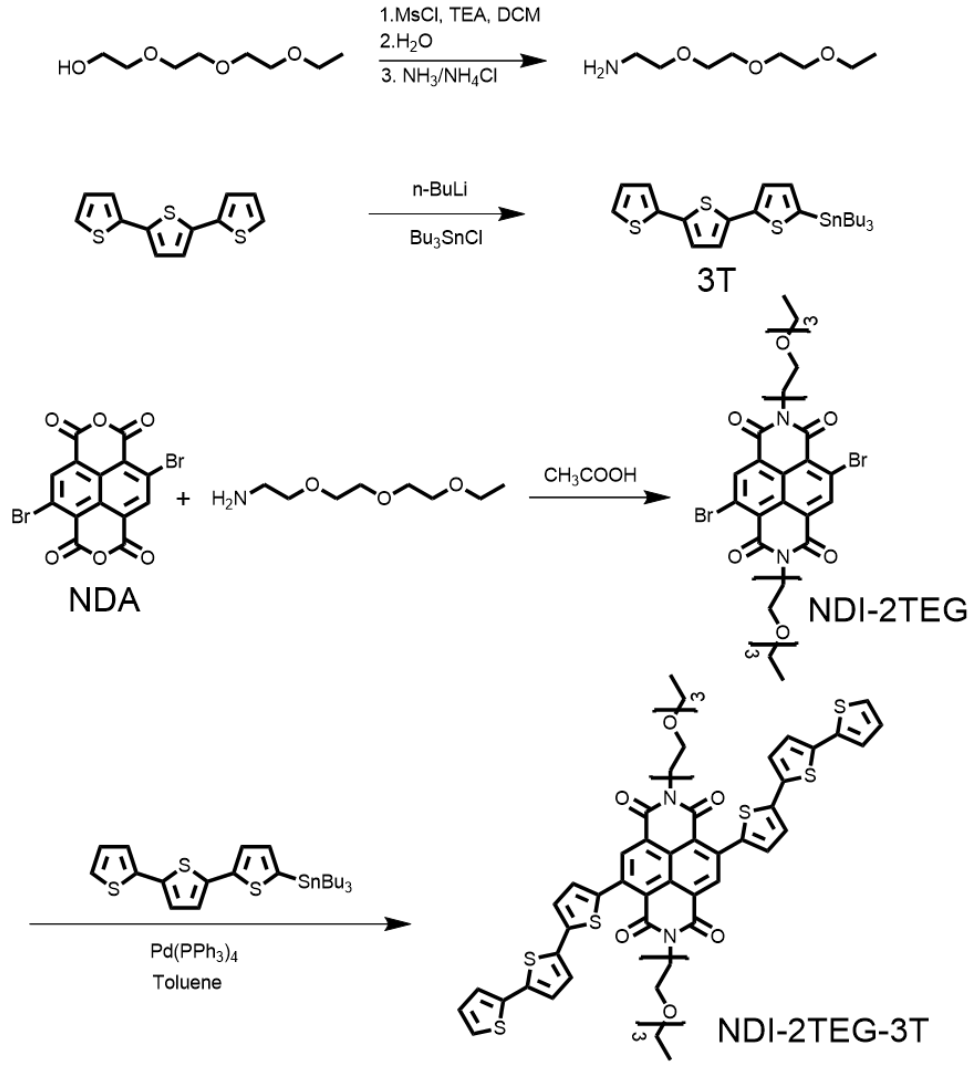

Figure S3.1: Synthetic route for NDI-2TEG-3T

4,9-dibromo-2,7-bis(2-(2-(2-ethoxyethoxy)ethoxy)ethyl)benzo[lmn][3,8]phenanthroline-1,3,6,8(2H,7H)-tetraone (**NDI-2TEG**) was synthesized according to literature procedures[51].

Synthesis of NDI-2TEG-3T

To a dry three-neck flask, NDI based monomer (**NDI-2TEG**) (20 mg, 0.027 mmol) and thiophene based monomer (**3T**) (60 mg, 0.1 mmol) were added under N_2 followed by catalyst Tetra(triphenylphosphine) palladium [$Pd(PPh_3)_4$] (8 mg). The flask and its contents were subjected to 3 pump/purge cycles with N_2 followed by addition of anhydrous, degassed

Toluene (5 mL) via syringe. The reaction mixture was stirred at 120 °C for overnight. After cooling to room temperature, the deeply colored reaction mixture was poured into 100 mL water, then extracted with CH_2Cl_2. The organic phase was washed with brine, dried over anhydrous sodium sulfate and removed solvent by rotary evaporator. The crude product was purified by silica gel column chromatography with CH_2Cl_2/acetone (20:1) as the eluent afforded 10 mg (34 % yield) target compound as solid.
^{1}HNMR (400 MHz, $CDCl_3$) δ: 8.78 (s, 2H), 7.30 (d, J = 3.7 Hz, 2H), 7.24 − 7.23 (m, 4H), 7.23 − 7.19 (m, 2H), 7.17 (d, J = 3.7 Hz, 2H), 7.12 (d, J = 3.7 Hz, 2H), 7.06 − 7.01 (m, 2H), 4.42 (t, J = 3.6 Hz, 4H), 3.91 − 3.77 (m, 4H), 3.77 − 3.65 (m, 4H), 3.65 − 3.56 (m, 8H), 3.54 − 3.42 (m, 8H), 1.15 (t, J = 3.6 Hz, 6H).
^{13}CNMR (100 MHz, $CDCl_3$) δ: 164.86, 164.84, 143.03, 142.07, 141.83, 139.80, 139.59, 139.18, 138.07, 132.90, 130.60, 130.27, 128.07, 127.76, 127.42, 127.11, 126.60, 126.54, 125.35, 73.34, 73.29, 72.79, 72.44, 70.54, 69.27, 42.42, 17.81.
HRMS(ESI) Calcd. for $C_{54}H_{51}N_2O_{10}S_6$ $[M+H]^+$: 1079.18625, found: 1079.18744; Calcd. for $C_{54}H_{54}N_3O_{10}S_6$ $[M+NH_4]^+$: 1096.21280, found: 1096.21404; Calcd. for $C_{54}H_{50}N_2O_{10}S_6Na_1$ $[M+Na]^+$: 1101.16819, found: 1101.16896.

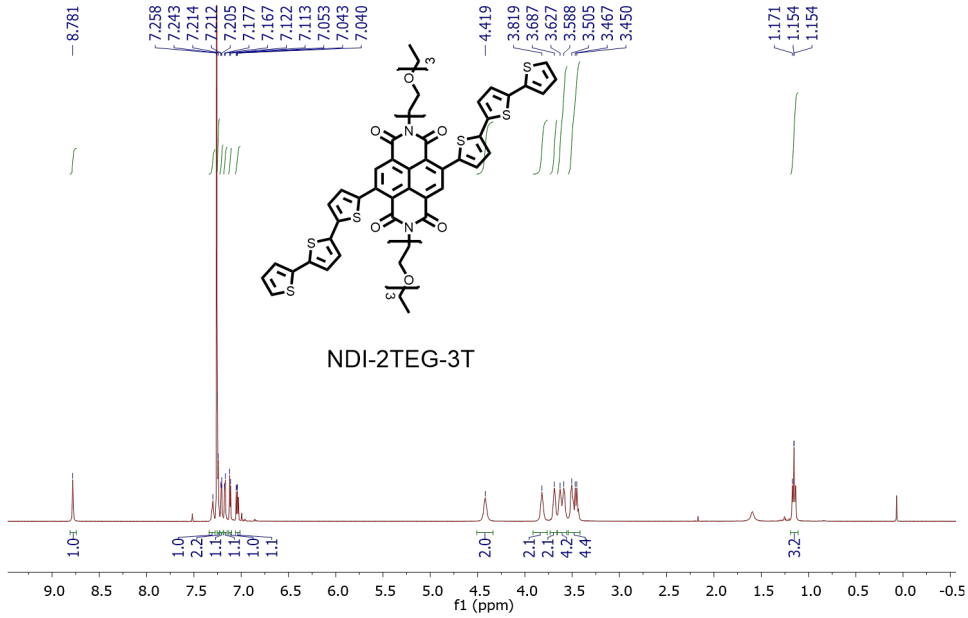

Figure S3.2: ^{1}HNMR spectrum of NDI-2TEG-3T.

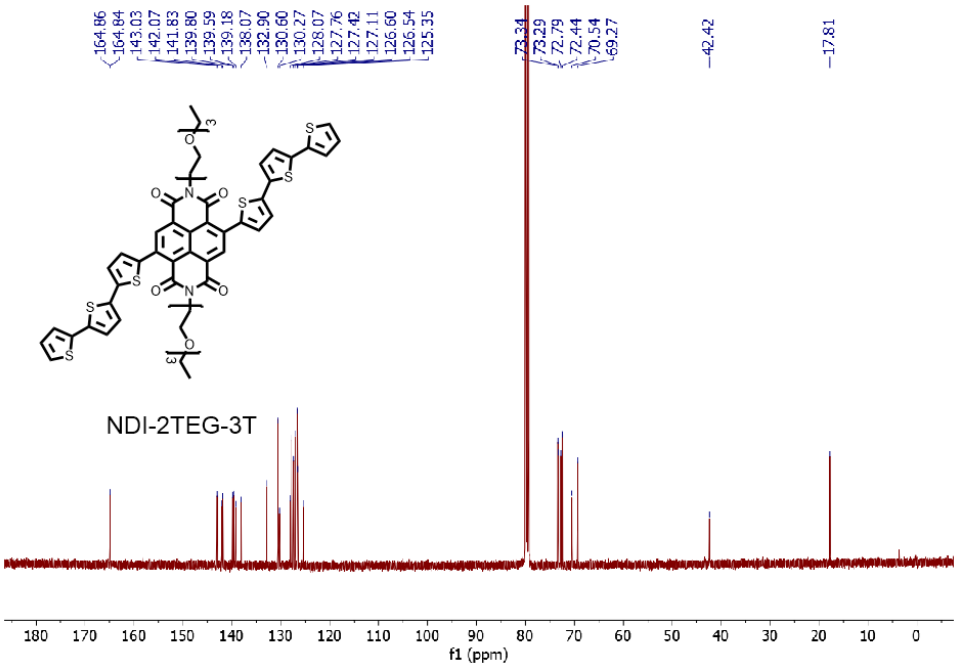

Figure S3.3: ^{13}CNMR spectrum of NDI-2TEG-3T.

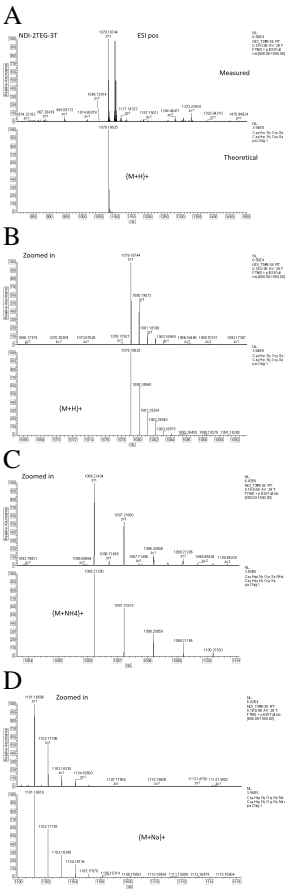

Figure S3.4: HRMS spectrum of NDI-2TEG-3T.

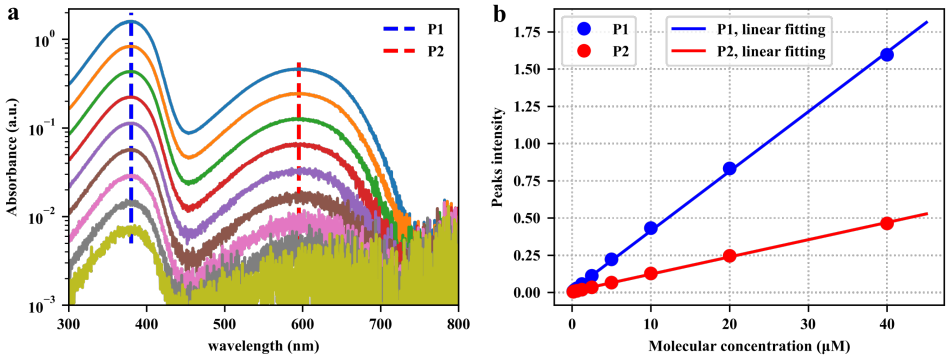

Figure S3.5: Absorption spectrum of NDI-2TEG-3T as a function of molecular concentration. The concentration of NDI-2TEG-3T was reduced by half at each step from top ($40\ \mu M$) to the bottom. Blue and red dashed lines represent the absorption peaks of the high-energy $\pi - \pi^*$ transition (P1) band and the low-energy intramolecular charge-transfer band (P2), respectively. (b) The two measured (dot) absorption peak intensities (P1 blue, P2 red) and their corresponding linear fits (solid lines) as functions of molecular concentration.

Fluorescence of NDI-2TEG-3T in Bulk

Quantum yield measurements of NDI-2TEG-3T

We estimated the quantum yield of NDI-2TEG-3T molecules by comparing their absorption and emission properties with commercial Alexa Fluor 647 dye, which has the quantum yield of 33%. Figure S3.6 gives the absorption and emission spectra of NDI-2TEG-3T (a) and Alexa Fluor 647 (b) in bulk solutions, respectively. The absorption spectra were recorded using a Cary 50 UV-Vis spectrometer (Varian Inc. Agilent Technology, USA), and the emission spectra were measured on a Cary Eclipse fluorescence spectrometer (Varian Inc. Agilent Technology, USA). The spectra for both NDI-2TEG-T3 and Alexa Fluor 647 were taken in the same experimental conditions, except that the solvent and molecular concentration were different. For Alexa Fluor 647, the molecular concentration was 290 nM in water, while for NDI-2TEG-T3, the molecules were dissolved in toluene with the concentration of 50 μM. In the plots, the spectra were normalized by the molecular concentration. As an approximation, we estimated the quantum yield of the NDI-2TEG-3T as,

$$Q_{\mathrm{NDI}} = Q_{\mathrm{Alexa647}} \cdot \frac{C_{\mathrm{Alexa647}}(\omega_{\mathrm{exc}}) < f_{\mathrm{NDI}} >}{C_{\mathrm{NDI}}(\omega_{\mathrm{exc}}) < f_{\mathrm{Alexa647}} >} \cdot \frac{n^2_{\mathrm{toluene}}}{n^2_{\mathrm{water}}}, \tag{S3.1}$$

from which we got the quantum yield of NDI-2TEG-3T, $Q_{\mathrm{NDI}} \approx 1.3 \times 10^{-4}$. Here, the subscripts "Alexa647" and "NDI" represent the Alexa Fluor 647 dye and NDI-2TEG-3T, respectively. C denotes the molecular absorption cross section. f_{NDI} and $f_{Alexa647}$ are the corresponding measured emission spectra, and $< \cdots >$ represents the averaging over the frequency. n_{toluene} and n_{water} are the refractive indices of toluene and water, respectively.

Average fluorescence intensity of an individual NDI-2TEG-3T molecule

To get the fluorescence enhancement factor, we measured the average brightness of NDI-2TEG-3T molecules in the focal volume without gold nanorods. The experimental conditions were the same as in the single-molecule enhancement measurement, except that the ex-

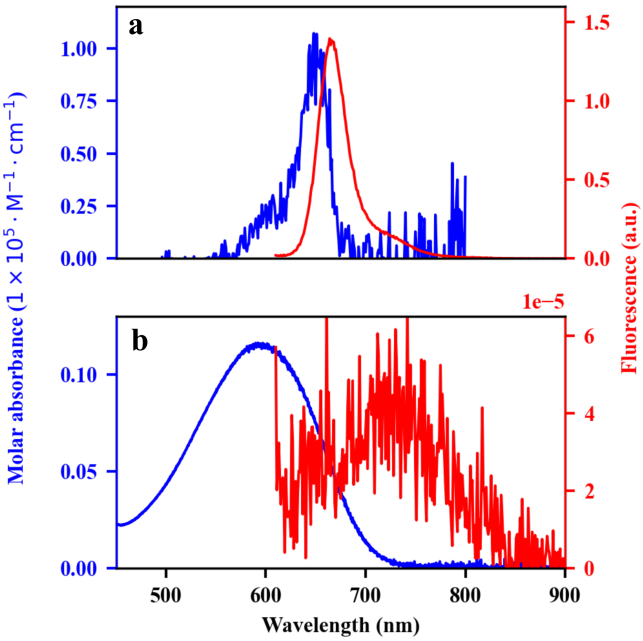

Figure S3.6: Fluorescence characterization of NDI-2TEG-3T. (a) Molecular absorption (blue) and emission (red) spectra of the commercial standard dye Alexa Fluor 647. (b) Molecular absorption (blue) and emission (red) spectra of NDI-2TEG-3T. The emission intensities were normalized with the corresponding molecular concentrations.

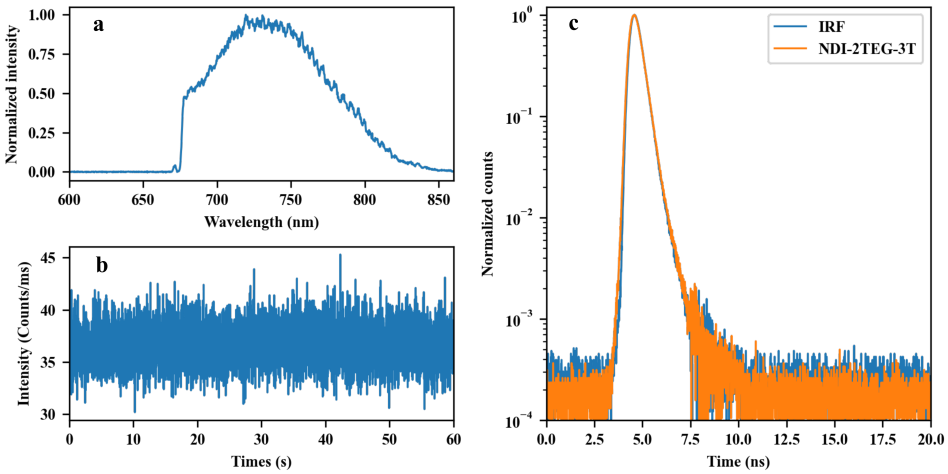

Figure S3.7: Non-enhanced fluorescence of NDI-2TEG-3T in the focal volume of the microscope. (a) Photoluminescence spectrum of NDI-2TEG-3T. (b) Photoluminescence time trace of non-enhanced molecules in the focal volume.(c) Lifetime histogram curve of NDI-2TEG-3T molecules (orange) in bulk solution. The lifetime of NDI-2TEG-3T is much shorter than the time resolution of our setup, as the curve is completely indistinguishable from the instrument response function (IRF, blue), which has an exponential decay with a time of about 0.38 ns.The molecular concentration of NDI-2TEG-3T was kept equal to 50 μM.

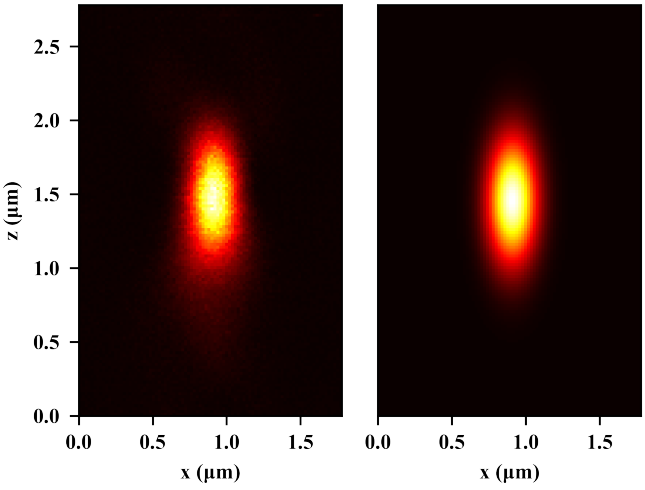

Figure S3.8: Left, XZ cross section of the scattering point spread function (PSF) with a gold nanorod. Right, two-dimensional Gaussian fit of the PSF, from which we get the widths of the PSF, $w_x = 0.24\,\mu$m and $w_z = 0.58\,\mu$m, and the PSF volume of 0.061 fL.

citation power was 3.3 times larger, and the concentration of molecules was higher. A $50\ \mu\mathrm{M}$ solution of NDI-2TEG-3T was excited with a $671\ \mathrm{nm}$ continuous wave (CW) laser (circularly polarized), and the fluorescence signal was separated from the background of scattered light by means of a long-pass filter ($\geq 675\ \mathrm{nm}$, LongPass U-Grade 671/RazorEdge, Semrock). The fluorescence intensity collected from the focal volume is depicted as time trace in Figure S3.7.b, and the corresponding emission spectrum of the non-enhanced molecules is shown in Figure S3.7.a. From the time trace, we got the average fluorescence intensity of about $36 \pm 6\ \mathrm{counts/ms}$. By considering that all the photoluminescence photons were due to the contribution of molecules in the focal volume, we got an estimated value of about $20 \pm 3\ \mathrm{counts/s}$ for the average intensity of each molecule. The focal volume is approximated by the volume of the point spread function of the microscope, which is about $0.061\ \mathrm{fL}$ (see Figure S3.8). Considering the difference in power, we estimated $6 \pm 1\ \mathrm{counts/s}$ the rate detected counts per molecule for the calculation of the enhancement factors.

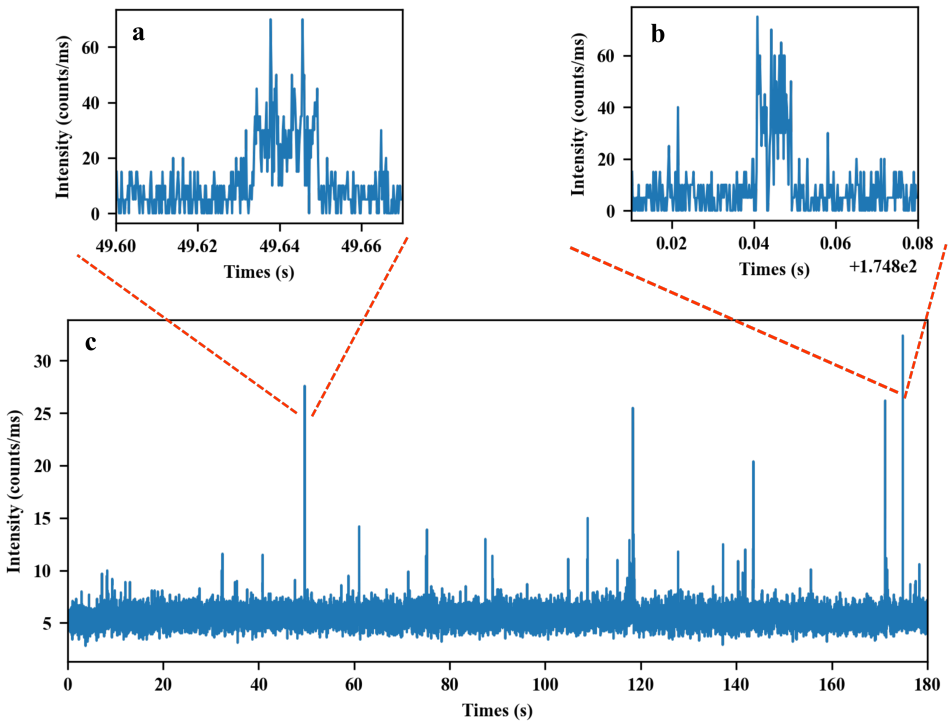

Figure S3.9: Single-molecule fluorescence enhancement by a gold nanorod. (c) Photoluminescence time trace with the binning time of 10 ms. (a, b) The zoomed views of the two highest bursts of the time trace in (a) with the binning time of 200 μs. The single-step intensity changes of these bursts confirm that the enhanced fluorescence signals are stemming from single molecules.

Single-molecule Fluorescence of NDI-2TEG-3T Enhanced by a Gold Nanorod.

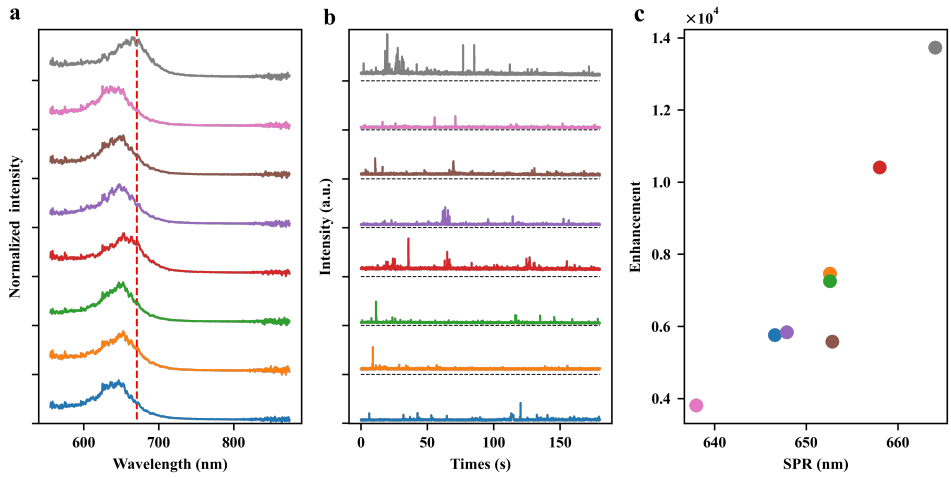

Figure S3.10: (a) Photoluminescence spectra of gold nanorods with different plasmon resonances. The red dashed line represents the excitation laser's wavelength of 671 nm. (b) The corresponding fluorescence time traces recorded on these gold nanorods, and (c) the maximum fluorescence enhancement as a function of the plasmon wavelength. The data recorded on every gold nanorod are indicated by their color in the plots. All time traces were recorded at the same molecular concentration of 1 μM.

S3.1.2. Theoretical Framework

Fluorescence enhancement simulations

In this paper, we follow the notations and definitions of Khatua et al. [24]. We consider the single molecule as a dipole $\mathbf{p_0}$ oscillating with frequency ω. As the theoretical absorption rate of the molecule is proportional to the intensity of the local field at its position, the excitation enhancement factor by a nanoantenna can be expressed as

$$\xi_{\mathrm{exc}} = \frac{I(\omega_{\mathrm{exc}})}{I_0(\omega_{\mathrm{exc}})} = \frac{|\mathbf{E}(\omega_{\mathrm{exc}})|^2}{|\mathbf{E}_0(\omega_{\mathrm{exc}})|^2}, \tag{S3.2}$$

where $\mathbf{E}(\omega_{\mathrm{exc}})$ and $\mathbf{E}_0(\omega_{\mathrm{exc}})$ are the electric fields at the position of the dipole with and without the nanoantenna, and ω_{exc} is the frequency of the illuminating light source. In the vicinity of the nanoantenna, the decay rate of the excited molecule is modified by coupling to the plasmon mode. On the basis of a simple two-level scheme, the emission factor can been expressed as[24]

$$\xi_{\mathrm{em}} = \xi_{\mathrm{rad}} \frac{\eta_0 C_{\mathrm{abs}} I_{\mathrm{exc}}/k_{\mathrm{r}}^0 + 1}{\xi_{\mathrm{exc}} \cdot \eta_0 C_{\mathrm{abs}} I_{\mathrm{exc}}/k_{\mathrm{r}}^0 + 1 + \eta_0(\xi_{\mathrm{rad}} + K_{\mathrm{nr}}/k_{\mathrm{r}}^0 - 1)}, \tag{S3.3}$$

here, I_{exc} is the intensity of the excitation wave, C_{abs} is the absorption cross section of the molecules, and $\xi_{\mathrm{rad}} = k_{\mathrm{r}}/k_{\mathrm{r}}^0$ is the radiative enhancement factor, which accounts for the increased local density of states in the vicinity of the antenna (Purcell effect [2, 52]). k_r and k_r^0 are the radiative decay rates with and without the nanoantenna, respectively, η_0 is the

intrinsic quantum yield of the emitter, and K_{nr} is the additional non-radiative absorption rate due to dissipative losses of the nanoantenna.

In Eq (S3.3), $\eta_0 C_{\mathrm{abs}} I_{\mathrm{exc}}$ accounts for the non-enhanced fluorescence rates of single molecules, which in our experiment is less than $10\ \mathrm{counts/s}$ (see previous section). From the simulations (see figure S3.11a.), the maximum radiative enhancement factor ($\xi_{\mathrm{rad,max}}$) and the additional non-radiative absorption rate ($K_{\mathrm{nr,max}}/k_{\mathrm{r}}^0$) are

$$\xi_{\mathrm{rad,max}} \sim 330, \tag{S3.4}$$

and

$$K_{\mathrm{nr,max}}/k_{\mathrm{r}}^0 \sim 4300. \tag{S3.5}$$

The intrinsic radiative rate of the molecules can be deduced from the quantum yield η_0 and the fluorescence lifetime τ_0 as $k_{\mathrm{r}}^0 = \eta_0/\tau_0$. For NDI-2TEG-3T, $\eta_0 \sim 1 \times 10^{-4}$ and $\tau_0 < 0.5\ \mathrm{ns}$. Therefore, we have

$$k_{\mathrm{r}}^0 > 2 \times 10^5\ \mathrm{s}^{-1}. \tag{S3.6}$$

From the discussion above, we find that, in our experiment conditions,

$$\eta_0 C_{\mathrm{abs}} I_{\mathrm{exc}}/k_{\mathrm{r}}^0 < 5 \times 10^{-5} \ll 1, \tag{S3.7}$$

and

$$\xi_{\mathrm{exc}} \eta_0 C_{\mathrm{abs}} I_{\mathrm{exc}}/k_{\mathrm{r}}^0 < 0.04 \ll \eta_0(\xi_{\mathrm{rad}} + K_{\mathrm{nr}}/k_{\mathrm{r}}^0 - 1) \sim 0.46, \tag{S3.8}$$

which means that the saturation of excitation is negligible. Therefore, the emission enhancement factor can been expressed as

$$\xi_{\mathrm{em}} = \frac{\xi_{\mathrm{rad}}}{1 + \eta_0(\xi_{\mathrm{rad}} + K_{\mathrm{nr}}/k_{\mathrm{r}}^0 - 1)}. \tag{S3.9}$$

In the discussions above, we have taken $0.5\ \mathrm{ns}$ as an upper bound for the NDI-2TEG-3T lifetime, which is in fact much shorter than the time resolution of our setup, as can be seen from the lifetime measurement in Figure S3.7.c. Therefore, in our experiment, we will be even further away from saturation than indicated by conditions of (S3.8), further supporting the simplified model of the emission enhancement factor in Eq (S3.9).

Consequently, the fluorescence intensity coming from the enhanced emitter is

$$I_{\mathrm{fluo}} = I_{\mathrm{exc}} \cdot C_{\mathrm{abs}} \cdot \eta_0 \cdot \xi_{\mathrm{exc}} \cdot \xi_{\mathrm{em}}. \tag{S3.10}$$

Considering the photoluminescence signal I_{GNR} of the gold nanorod as the only source of background, we can define the signal-to-noise ratio of the coupled system between the emitter and the gold nanorod as

$$S/N = I_{\mathrm{fluo}} \cdot \Delta t/\sqrt{I_{\mathrm{GNR}} \cdot \Delta t}, \tag{S3.11}$$

where Δt is the binning time for single-photon counting, supposing the signal to remain constant during the acquisition time.

To evaluate the enhancement factor by a single gold nanorod numerically, we applied a classical electrodynamics approach based on a boundary element method (SCUFF-EM)

to simulate the excitation and emission enhancement, respectively [53, 54]. To get the excitation enhancement, we assumed the gold nanorod is excited by a plane wave, while for the decay rates, we modeled the excited emitter as a radiating dipole, whose time-averaged radiated power in a medium without nanorod is

$$P_{r0}(\omega) = \frac{|\mathbf{p}_0|^2}{4\pi\varepsilon_0}\frac{n\omega^4}{3c^3}, \tag{S3.12}$$

where n is the refractive index of the medium, c is the speed of light and ε_0 is the vacuum permittivity. The enhancement factor of radiative rates (ξ_{rad}) and the non-radiative dissipation rate (K_{nr}) by the nanoantenna were derived from

$$\xi_{\mathrm{rad}} = k_{\mathrm{r}}/k_{\mathrm{r}}^0 = P_{\mathrm{rad}}/P_{\mathrm{r0}}, \tag{S3.13}$$

and

$$K_{\mathrm{nr}}/k_{\mathrm{r}}^0 = P_{\mathrm{abs}}/P_{\mathrm{r0}}. \tag{S3.14}$$

In the simulations, the power absorbed by the gold nanorod P_{abs} was calculated by integrating the Poynting vector over the nanorod surface, which was modeled as a spherically capped cylinder, and the radiated power P_{rad} was obtained from

$$P_{\mathrm{rad}}(\omega) + P_{\mathrm{abs}}(\omega) = \frac{\omega^3}{2c^2\varepsilon_0}|\mathbf{p}_0|^2[\mathbf{n}\cdot\mathrm{Im}[\mathbf{G}(\mathbf{r},\mathbf{r};\omega)]\cdot\mathbf{n}], \tag{S3.15}$$

where $\mathbf{G}(\mathbf{r},\mathbf{r};\omega)$ is the Green tensor at the emitter's position $\mathbf{r}$ and $\mathbf{n}$ represents the direction of the dipole moment[55].

From Eqs. (S3.12) and (S3.15), we can clearly see that the radiative rate enhancement ($\xi_{\mathrm{rad}}^{\omega}$) and the non-radiative relaxation rate $K_{\mathrm{nr}}^{\omega}(\omega)$ both depend on the frequency of the emitted photons (ω). To get the emission enhancement for all the photons, we calculate the average radiative rate enhancement and non-radiative relaxation rate:

$$\xi_{\mathrm{rad}} = \int \xi_{\mathrm{rad}}^{\omega}(\omega)F_{\mathrm{dye}}(\omega)d\omega, \tag{S3.16}$$

$$K_{\mathrm{nr}} = \int K_{\mathrm{nr}}^{\omega}(\omega)F_{\mathrm{dye}}(\omega)d\omega, \tag{S3.17}$$

here, $F_{\mathrm{dye}}(\omega)$ is the normalized emission spectra of the molecule and $\int F_{\mathrm{dye}}(\omega)d\omega = 1$.

Dependence of the Emission Enhancement on the Gap and on the Quantum Yield

The simple cube root dependence of the optimal gap on the quantum yield (Fig S3.11c.) can be explained briefly as followed. At a given quantum yield, considering the emission enhancement factor as a function of the gap, the derivative of Eq (S3.9) at the optimal gap d_{m} gives

$$\frac{d\xi_{\mathrm{em}}}{d(\mathrm{gap})}\Big|_{\mathrm{gap=d_m}} = \frac{d}{d(\mathrm{gap})}\left[\frac{\xi_{\mathrm{rad}}}{1+\eta_0(\xi_{\mathrm{rad}}+K_{\mathrm{nr}}/k_{\mathrm{r}}^0-1)}\right]\Bigg|_{\mathrm{gap=d_m}} = 0, \tag{S3.18}$$

from which we can get a relationship between the quantum yield and the optimal gaps as,

$$\eta_0 = \frac{1}{\frac{\xi_{\mathrm{rad}}}{\xi'_{\mathrm{rad}}} K'_{\mathrm{nr}}/k^0_{\mathrm{r}} - K_{\mathrm{nr}}/k^0_{\mathrm{r}} + 1}, \tag{S3.19}$$

here, $\xi'_{\mathrm{rad}} = \frac{d}{d(\mathrm{gap})}\xi_{\mathrm{rad}}(\mathrm{gap})\big|_{\mathrm{gap}=\mathrm{d_m}}$ and $K'_{\mathrm{nr}} = \frac{d}{d(\mathrm{gap})}K_{\mathrm{nr}}(\mathrm{gap})\big|_{\mathrm{gap}=\mathrm{d_m}}$.

Considering the simplest power dependence of the enhanced radiative and nonradiative rates on the gap: $\xi_{\mathrm{rad}}(\mathrm{gap}) \propto \mathrm{gap}^{-\alpha}$ and $K_{\mathrm{nr}}(\mathrm{gap})/k^0_{\mathrm{r}} \propto \mathrm{gap}^{-\beta}$, Eq (S3.19) can be expressed as

$$\eta_0 = \frac{1}{(\beta/\alpha - 1)K_{\mathrm{nr}}/k^0_{\mathrm{r}} + 1} \approx \frac{1}{(\beta/\alpha - 1)}(K_{\mathrm{nr}}/k^0_{\mathrm{r}})^{-1} \propto {\mathrm{d_m}}^{\beta}, \tag{S3.20}$$

from this, we get the power law approximation for the optimal gap: $\mathrm{d_m} \propto \eta_0^{1/\beta}$. Here $\beta > \alpha$, because the enhanced non-radiative rates decreases more rapidly than the radiative rates as the molecules move away from the metal surface(Figure S3.11.a). The decay rate β can vary from 3 to 6[56], depending on the geometric configuration of the coupling system, such as the surface curvature of the particle, the position and orientation of the molecules et al. In our case, for the typical size of gold nanorod, we find that $\beta \sim 3$ gives a good approximation (Figure S3.11), therefore $\mathrm{d_m} \propto \eta_0^{1/3}$.

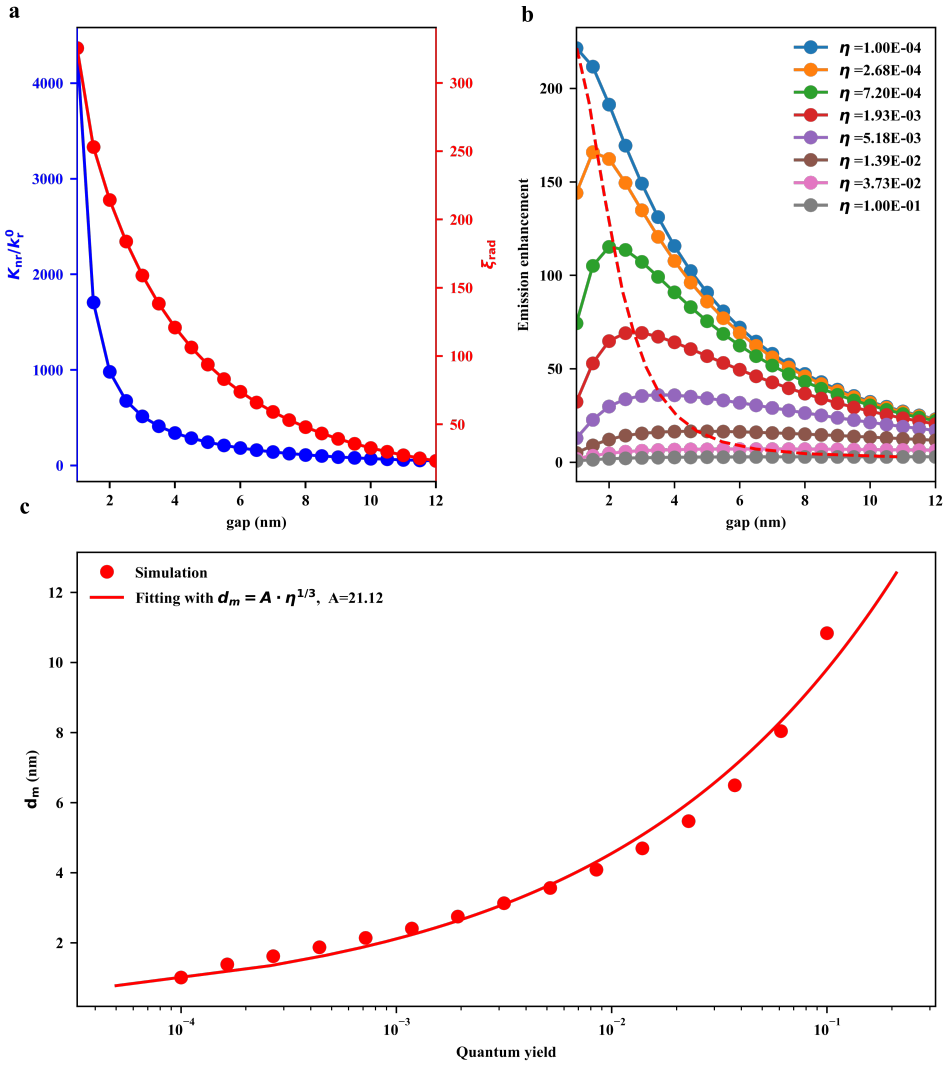

Figure S3.11: (a) Radiative rate enhancement factor (red) and additional non-radiative rate (blue) as functions of the gap. (b) Emission enhancement as a function of the gap for the molecules with different quantum yields. Red dashed line indicates the maximum emissions of different quantum yields. (c) The corresponding positions (d_m) of maximum emission enhancements for different quantum yields. Here, we find that the quantum yield dependence of the optimal distance can be approximated by a very simple power law as $d_\mathrm{m} \propto \eta^{\frac{1}{3}}$.

Dual-Lorentzian Model for Fluorescence Enhancement by a Gold Nanorod

In order to quickly optimize plasmon enhanced fluorescence without performing time consuming fullwave-simulation, we can apply a dual-Lorentzian model to the gold nanorod-emitter system for the molecules with very low quantum yields. As we can see from Eq (S3.9), the emission enhancement ξ_{em} reduces to the radiative enhancement ξ_{rad} for vanishing quantum yields:

$$\xi_{\mathrm{em}} \sim \xi_{\mathrm{rad}}[1-\eta_0(\xi_{\mathrm{rad}}+K_{\mathrm{nr}}/k_{\mathrm{r}}^0-1)] \xrightarrow{\eta_0\to 0} \xi_{\mathrm{rad}}, \tag{S3.21}$$

The emission enhancement factor ξ_{rad} depends on the frequency (ω) of the emitted photon and on the plasmon frequency (ω_{sp}) of the nanorod and can be expressed as an integral over all emitted photons (as in Eq. (S3.16)):

$$\xi_{\mathrm{em,avg}}(\omega_{\mathrm{sp}}) \sim \int \xi_{\mathrm{rad}}^{\omega}(\omega_{\mathrm{sp}},\omega)F_{\mathrm{dye}}(\omega)d\omega. \tag{S3.22}$$

Substituting this Eq. (S3.22) into the Eq. (S3.10), we can estimate the enhanced fluorescence intensity from the molecule, which is linearly dependent on the molecular absorption spectrum and emission, and the plasmon response of the gold nanorod (represented by the enhancement factors of excitation and radiative rates),

$$\begin{aligned} I_{fluo}(\omega_{\mathrm{exc}},\omega_{\mathrm{sp}}) &= I_{\mathrm{exc}}\cdot C_{\mathrm{abs}}(\omega_{\mathrm{exc}})\cdot\eta_0\cdot\xi_{\mathrm{exc}}(\omega_{\mathrm{exc}},\omega_{\mathrm{sp}})\cdot\xi_{\mathrm{em,avg}}(\omega_{\mathrm{sp}}) \\ &\sim I_{\mathrm{exc}}\cdot\eta_0\cdot\int C_{\mathrm{abs}}(\omega_{\mathrm{exc}})\cdot\underbrace{[\xi_{\mathrm{exc}}(\omega_{\mathrm{exc}},\omega_{\mathrm{sp}})\cdot\xi_{\mathrm{rad}}^{\omega}(\omega_{\mathrm{sp}},\omega)]}_{\text{plasmon response}}\cdot F_{\mathrm{dye}}(\omega)d\omega. \end{aligned} \tag{S3.23}$$

As a result of the square dependence on the near-field, both the enhanced excitation and emission rates, $\xi_{\mathrm{ext}}(\omega_{exc},\omega_{\mathrm{sp}})$ and $\xi_{\mathrm{rad}}(\omega_{\mathrm{sp}},\omega)$, have similar lineshapes as the spectra of the the gold nanorod plasmon resonance, all of which can be expressed by using the same Lorentzian lineshape

$$\xi_{[\mathrm{exc,rad}]}(\omega_i,\omega_{\mathrm{sp}}) \sim L_{[\mathrm{exc,rad}]}(\omega_{\mathrm{sp}})\cdot\frac{\Gamma/2}{(\omega_i-\omega_{\mathrm{sp}})^2+(\Gamma/2)^2}, \tag{S3.24}$$

where, Γ is the width of the plasmon resonance, ω_i represents the frequencies of excitation, emission, or scattering photons by the nanorod. $L_{[\mathrm{exc,rad}]}(\omega_{\mathrm{sp}})$ is the normalization factor, which depends on plasmon wavelengths of the nanorods. Simply, we can set $L_{\mathrm{rad}}(\omega_{\mathrm{sp}})$ as a constant, and $L_{\mathrm{exc}}(\omega_{\mathrm{sp}}) \propto C_{\mathrm{sca}}(\omega_{\mathrm{sp}})$. Here $C_{\mathrm{sca}}(\omega_{\mathrm{sp}})$ is the scattering cross section of the nanorod at resonance wavelength, which can be easily calculated by using Mie-Gans theory (green dashed line in Figure S3.12)[57].

From Eq. (S3.23) and Eq. (S3.24), we can get a quick estimation of the dependence of the enhancement factors and the fluorescence intensity on wavelengths of the excitation and of the plasmon resonance, by simply considering the spectral overlap of the molecular absorption and emission and the square of Lorentzian lineshape of the plasmon resonance. This simplified form allows us to select the best experimental condition to get maximum intensity without the need for time-consuming fullwave-simulations. As an example, in our case we got $\omega_{\mathrm{exc}} = 669$ nm and $\omega_{\mathrm{sp}} = 674$ nm, which is very close to the full-wave simulation result as shown in Figure 1.c in the main text. The detailed comparison of the

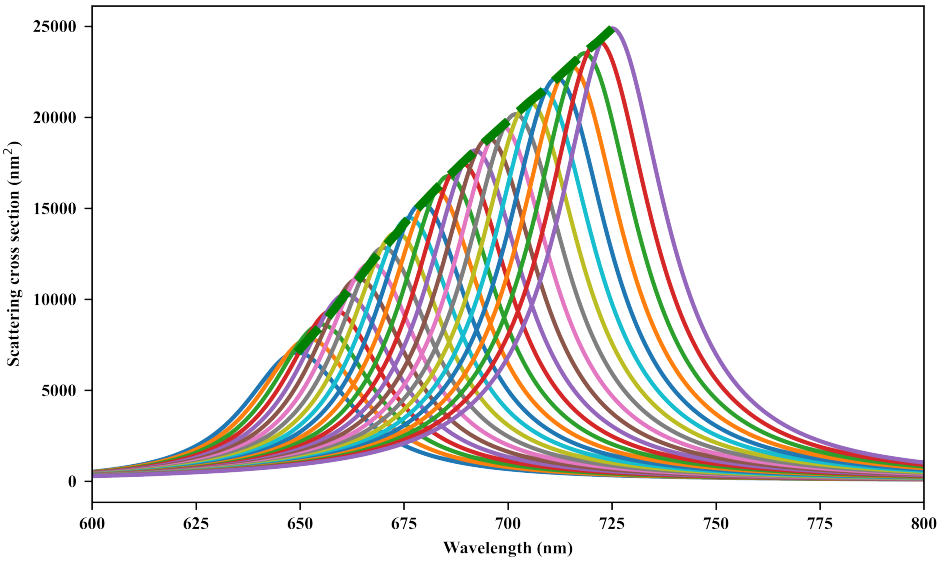

Figure S3.12: Scattering cross section of gold nanorods with the same diameter but with different aspect ratios. The green dashed line gives the values at the resonance wavelengths, which are proportional to normalization factors $L_{\mathrm{exc}}(\omega_{\mathrm{sp}})$ in Eq. (S3.24). The cross sections were calculated by using Mie-Gans theory, where the diameter of the gold nanorods was a constant set as 25 nm.

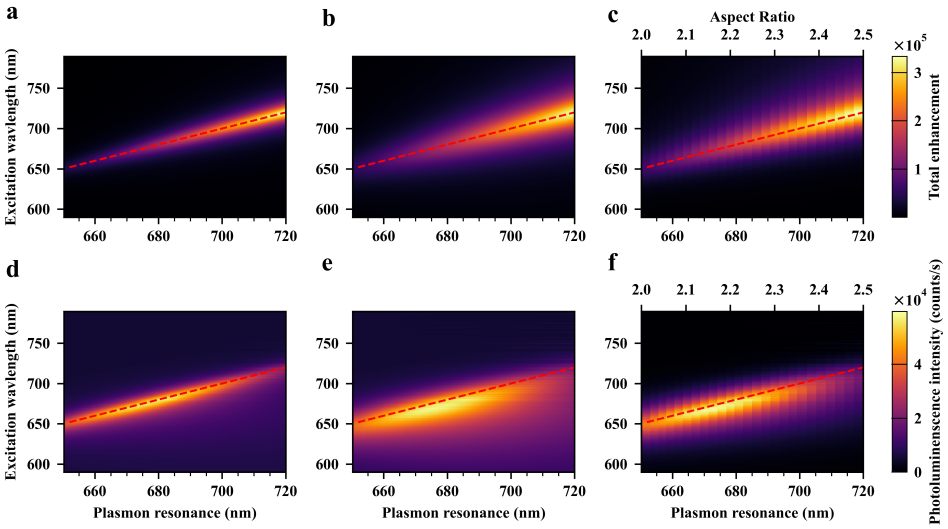

Figure S3.13: Dual-Lorentzian model for gold nanorod-emitter system. (a, b, c) are the total fluorescence enhancement as a function of excitation wavelength and plasmon wavelength of the gold nanorod, (d, e, f) are the corresponding fluorescence intensities. Here, (a, d) correspond to the Lorentzian model with the FWHM of 20 nm, (b, e) correspond to FWHM of 40 nm, and (c, f) were calculated with full-wave simulations.

full-wave simulation and the models with different full width at half maximum (FWHM) of the gold nanorod plasmon is shown in Figure S3.13. From the Figure S3.13.(e, f), we can see that the “sweet spot" for the optimized fluorescence is the same for the wavelengths of the excitation and plasmon. We should mention here, as we can see in Figure S3.13.(b,c), that the optimized wavelengths of excitation and plasmon to get maximum total enhancement are much red-shifted compared to the fluorescence intensity, due to the large Stokes shift ($3,000\ \mathrm{cm}^{-1}$) of the molecule.

References

[1] C. Zander, J. Enderlein, and R. A. Keller. *Single-molecule detection in solution—methods and applications.* VCH-Wiley, 2002.

[2] Guowei Lu, Tianyue Zhang, Wenqiang Li, Lei Hou, Jie Liu, and Qihuang Gong. Single-Molecule Spontaneous Emission in the Vicinity of an Individual Gold Nanorod. *The Journal of Physical Chemistry C*, 115(32):15822–15828, August 2011.

[3] W. Ho. Single-molecule chemistry. *The Journal of Chemical Physics*, 117(24):11033–11061, December 2002.

[4] Denis Garoli, Hirohito Yamazaki, Nicolò Maccaferri, and Meni Wanunu. Plasmonic Nanopores for Single-Molecule Detection and Manipulation: Toward Sequencing Applications. *Nano Letters*, 19(11):7553–7562, November 2019.

[5] Aleksandr Barulin, Jean-Benoît Claude, Satyajit Patra, Nicolas Bonod, and Jérôme Wenger. Deep Ultraviolet Plasmonic Enhancement of Single Protein Autofluorescence in Zero-Mode Waveguides. *Nano Letters*, 19(10):7434–7442, October 2019.

[6] W. E. Moerner and L. Kador. Optical detection and spectroscopy of single molecules in a solid. *Physical Review Letters*, 62(21):2535–2538, May 1989.

[7] W. E. Moerner and Michel Orrit. Illuminating Single Molecules in Condensed Matter. *Science*, 283(5408):1670–1676, March 1999.

[8] W. E. (William E.) Moerner. Nobel Lecture: Single-molecule spectroscopy, imaging, and photocontrol: Foundations for super-resolution microscopy. *Reviews of Modern Physics*, 87(4):1183–1212, October 2015.

[9] M. Orrit and J. Bernard. Single pentacene molecules detected by fluorescence excitation in a p-terphenyl crystal. *Physical Review Letters*, 65(21):2716–2719, November 1990.

[10] Taekjip Ha. Single-Molecule Fluorescence Resonance Energy Transfer. *Methods*, 25(1):78–86, September 2001.

[11] Richard A. Keller, W. Patrick Ambrose, Peter M. Goodwin, James H. Jett, John C. Martin, and Ming Wu. Single-Molecule Fluorescence Analysis in Solution. *Applied Spectroscopy*, 50(7):12A–32A, July 1996.

[12] W. E. Moerner and David P. Fromm. Methods of single-molecule fluorescence spectroscopy and microscopy. *Review of Scientific Instruments*, 74(8):3597–3619, August 2003.

[13] Pascal Anger, Palash Bharadwaj, and Lukas Novotny. Enhancement and Quenching of Single-Molecule Fluorescence. *Physical Review Letters*, 96(11):113002, March 2006.

[14] Joseph R Lakowicz. *Principles of fluorescence spectroscopy*. Springer Science & Business Media, 2013.

[15] Jeff W. Lichtman and José-Angel Conchello. Fluorescence microscopy. *Nature Methods*, 2(12):910–919, December 2005.

[16] Jianhong Chen, Weimin Liu, Bingjiang Zhou, Guangle Niu, Hongyan Zhang, Jiasheng Wu, Ying Wang, Weigang Ju, and Pengfei Wang. Coumarin- and Rhodamine-Fused Deep Red Fluorescent Dyes: Synthesis, Photophysical Properties, and Bioimaging in Vitro. *The Journal of Organic Chemistry*, 78(12):6121–6130, June 2013.

[17] Melari Davies, Christophe Jung, Philipp Wallis, Tobias Schnitzler, Chen Li, Klaus Müllen, and Christoph Bräuchle. Photophysics of New Photostable Rylene Derivatives: Applications in Single-Molecule Studies and Membrane Labelling. *ChemPhysChem*, 12(8):1588–1595, 2011.

[18] BR Henry and W Siebrand. Organic molecular photophysics. *by JB Birks, Wiley, New York*, 1:153, 1973.

[19] Jord C. Prangsma, Robert Molenaar, Laura van Weeren, Daphne S. Bindels, Lindsay Haarbosch, Jente Stouthamer, Theodorus W. J. Gadella, Vinod Subramaniam, Willem L. Vos, and Christian Blum. Quantitative Determination of Dark Chromophore Population Explains the Apparent Low Quantum Yield of Red Fluorescent Proteins. *The Journal of Physical Chemistry B*, 124(8):1383–1391, February 2020.

[20] Kateryna S. Morozova, Kiryl D. Piatkevich, Travis J. Gould, Jinghang Zhang, Joerg Bewersdorf, and Vladislav V. Verkhusha. Far-Red Fluorescent Protein Excitable with Red Lasers for Flow Cytometry and Superresolution STED Nanoscopy. *Biophysical Journal*, 99(2):L13–L15, July 2010.

[21] Daria M. Shcherbakova and Vladislav V. Verkhusha. Near-infrared fluorescent proteins for multicolor in vivo imaging. *Nature Methods*, 10(8):751–754, August 2013.

[22] Sergei Kühn, Ulf Håkanson, Lavinia Rogobete, and Vahid Sandoghdar. Enhancement of Single-Molecule Fluorescence Using a Gold Nanoparticle as an Optical Nanoantenna. *Physical Review Letters*, 97(1):017402, July 2006.

[23] Paolo Ponzellini, Xavier Zambrana-Puyalto, Nicolò Maccaferri, Luca Lanzanò, Francesco De Angelis, and Denis Garoli. Plasmonic zero mode waveguide for highly confined and enhanced fluorescence emission. *Nanoscale*, 10(36):17362–17369, September 2018.

[24] Saumyakanti Khatua, Pedro M. R. Paulo, Haifeng Yuan, Ankur Gupta, Peter Zijlstra, and Michel Orrit. Resonant Plasmonic Enhancement of Single-Molecule Fluorescence by Individual Gold Nanorods. *ACS Nano*, 8(5):4440–4449, May 2014.

[25] Haifeng Yuan, Saumyakanti Khatua, Peter Zijlstra, Mustafa Yorulmaz, and Michel Orrit. Thousand-fold Enhancement of Single-Molecule Fluorescence Near a Single Gold Nanorod. *Angewandte Chemie International Edition*, 52(4):1217–1221, 2013.

[26] Saumyakanti Khatua, Haifeng Yuan, and Michel Orrit. Enhanced-fluorescence correlation spectroscopy at micro-molar dye concentration around a single gold nanorod. *Physical Chemistry Chemical Physics*, 17(33):21127–21132, August 2015.

[27] Deep Punj, Mathieu Mivelle, Satish Babu Moparthi, Thomas S. van Zanten, Hervé Rigneault, Niek F. van Hulst, María F. García-Parajó, and Jérôme Wenger. A plasmonic 'antenna-in-box' platform for enhanced single-molecule analysis at micromolar concentrations. *Nature Nanotechnology*, 8(7):512–516, July 2013.

[28] Deep Punj, Juan de Torres, Hervé Rigneault, and Jérôme Wenger. Gold nanoparticles for enhanced single molecule fluorescence analysis at micromolar concentration. *Optics Express*, 21(22):27338–27343, November 2013.

[29] Valentin Flauraud, Raju Regmi, Pamina M. Winkler, Duncan T. L. Alexander, Hervé Rigneault, Niek F. van Hulst, María F. García-Parajo, Jérôme Wenger, and Jürgen Brugger. In-Plane Plasmonic Antenna Arrays with Surface Nanogaps for Giant Fluorescence Enhancement. *Nano Letters*, 17(3):1703–1710, March 2017.

[30] Anastasiya Puchkova, Carolin Vietz, Enrico Pibiri, Bettina Wünsch, María Sanz Paz, Guillermo P. Acuna, and Philip Tinnefeld. DNA Origami Nanoantennas with over 5000-fold Fluorescence Enhancement and Single-Molecule Detection at 25 μM. *Nano Letters*, 15(12):8354–8359, December 2015.

[31] Anika Kinkhabwala, Zongfu Yu, Shanhui Fan, Yuri Avlasevich, Klaus Müllen, and W. E. Moerner. Large single-molecule fluorescence enhancements produced by a bowtie nanoantenna. *Nature Photonics*, 3(11):654–657, November 2009.

[32] Anika A. Kinkhabwala, Zongfu Yu, Shanhui Fan, and W. E. Moerner. Fluorescence correlation spectroscopy at high concentrations using gold bowtie nanoantennas. *Chemical Physics*, 406:3–8, October 2012.

[33] Peter Zijlstra, Pedro M. R. Paulo, and Michel Orrit. Optical detection of single non-absorbing molecules using the surface plasmon resonance of a gold nanorod. *Nature Nanotechnology*, 7(6):379–382, June 2012.

[34] Leonid Vigderman, Bishnu P. Khanal, and Eugene R. Zubarev. Functional Gold Nanorods: Synthesis, Self-Assembly, and Sensing Applications. *Advanced Materials*, 24(36):4811–4841, 2012.

[35] Huanjun Chen, Lei Shao, Qian Li, and Jianfang Wang. Gold nanorods and their plasmonic properties. *Chemical Society Reviews*, 42(7):2679–2724, March 2013.

[36] Joseph R. Lakowicz. Radiative decay engineering 5: Metal-enhanced fluorescence and plasmon emission. *Analytical Biochemistry*, 337(2):171–194, February 2005.

[37] O. L. Muskens, V. Giannini, J. A. Sánchez-Gil, and J. Gómez Rivas. Strong Enhancement of the Radiative Decay Rate of Emitters by Single Plasmonic Nanoantennas. *Nano Letters*, 7(9):2871–2875, September 2007.

[38] R. Carminati, J. J. Greffet, C. Henkel, and J. M. Vigoureux. Radiative and non-radiative decay of a single molecule close to a metallic nanoparticle. *Optics Communications*, 261(2):368–375, May 2006.

[39] David Canevet, Marc Sallé, Guanxin Zhang, Deqing Zhang, and Daoben Zhu. Tetrathiafulvalene (TTF) derivatives: Key building-blocks for switchable processes. *Chemical Communications*, (17):2245–2269, April 2009.

[40] Yanlin Chen, Xianfeng Liang, Haiyan Yang, Qin Wang, Xubing Zhou, De Guo, Shayu Li, Cailong Zhou, Lichun Dong, Zitong Liu, Zhengxu Cai, Wei Chen, and Luxi Tan. Strong Near-Infrared Solid Emission and Enhanced N-Type Mobility for Poly(naphthalene Diimide) Vinylene by a Random Polymerization Strategy. *Macromolecules*, 52(21):8332–8338, November 2019.

[41] P. B. Johnson and R. W. Christy. Optical Constants of the Noble Metals. *Physical Review B*, 6(12):4370–4379, December 1972.

[42] E. Dulkeith, A. C. Morteani, T. Niedereichholz, T. A. Klar, J. Feldmann, S. A. Levi, F. C. J. M. van Veggel, D. N. Reinhoudt, M. Möller, and D. I. Gittins. Fluorescence Quenching of Dye Molecules near Gold Nanoparticles: Radiative and Nonradiative Effects. *Physical Review Letters*, 89(20):203002, October 2002.

[43] Fabio Cannone, Giuseppe Chirico, Anna Rita Bizzarri, and Salvatore Cannistraro. Quenching and Blinking of Fluorescence of a Single Dye Molecule Bound to Gold Nanoparticles. *The Journal of Physical Chemistry B*, 110(33):16491–16498, August 2006.

[44] Sinisa Vukovic, Stefano Corni, and Benedetta Mennucci. Fluorescence Enhancement of Chromophores Close to Metal Nanoparticles. Optimal Setup Revealed by the Polarizable Continuum Model. *The Journal of Physical Chemistry C*, 113(1):121–133, January 2009.

[45] Martín Caldarola, Biswajit Pradhan, and Michel Orrit. Quantifying fluorescence enhancement for slowly diffusing single molecules in plasmonic near fields. *The Journal of Chemical Physics*, 148(12):123334, March 2018.

[46] Biswajit Pradhan, Saumyakanti Khatua, Ankur Gupta, Thijs Aartsma, Gerard Canters, and Michel Orrit. Gold-Nanorod-Enhanced Fluorescence Correlation Spectroscopy of Fluorophores with High Quantum Yield in Lipid Bilayers. *The Journal of Physical Chemistry C*, 120(45):25996–26003, November 2016.

[47] A. Mooradian. Photoluminescence of Metals. *Physical Review Letters*, 22(5):185–187, February 1969.

[48] Weichun Zhang, Martín Caldarola, Xuxing Lu, Biswajit Pradhan, and Michel Orrit. Single-molecule fluorescence enhancement of a near-infrared dye by gold nanorods using DNA transient binding. *Physical Chemistry Chemical Physics*, 20(31):20468–20475, August 2018.

[49] Eilaf Ahmed, Guoqiang Ren, Felix S. Kim, Emily C. Hollenbeck, and Samson A. Jenekhe. Design of New Electron Acceptor Materials for Organic Photovoltaics: Synthesis, Electron Transport, Photophysics, and Photovoltaic Properties of Oligothiophene-Functionalized Naphthalene Diimides. *Chemistry of Materials*, 23(20):4563–4577, October 2011.

[50] Dávid Komáromy, Marc C. A. Stuart, Guillermo Monreal Santiago, Meniz Tezcan, Victor V. Krasnikov, and Sijbren Otto. Self-Assembly Can Direct Dynamic Covalent Bond Formation toward Diversity or Specificity. *Journal of the American Chemical Society*, 139(17):6234–6241, May 2017.

[51] Heather F. Higginbotham, Subashani Maniam, Steven J. Langford, and Toby D. M. Bell. New brightly coloured, water soluble, core-substituted naphthalene diimides for biophysical applications. *Dyes and Pigments*, 112:290–297, January 2015.

[52] Anonymous. Proceedings of the American Physical Society. *Physical Review*, 69(11-12):674–674, June 1946.

[53] M. T. Homer Reid and Steven G. Johnson. Efficient Computation of Power, Force, and Torque in BEM Scattering Calculations. *IEEE Transactions on Antennas and Propagation*, 63(8):3588–3598, August 2015.

[54] `http://github.com/homerreid/scuff-EM`.

[55] Lukas Novotny and Bert Hecht. *Principles of Nano-Optics*. Cambridge University Press, 2006.

[56] Maxim Sukharev, Noa Freifeld, and Abraham Nitzan. Numerical Calculations of Radiative and Non-Radiative Relaxation of Molecules Near Metal Particles. *The Journal of Physical Chemistry C*, 118(20):10545–10551, May 2014.

[57] R v Gans. Über die form ultramikroskopischer silberteilchen. *Annalen der Physik*, 352(10):270–284, 1915.